BUTTERWORTH HEINEMANN

Polymer Vol. 36 No. 9, pp. 1761–1779, 1995
Elsevier Science Ltd
Printed in Great Britain

Low-voltage, high-resolution scanning electron microscopy: a new characterization technique for polymer morphology*

Deborah L. Vezie and Edwin L. Thomas†
Department of Materials Science and Engineering, Massachusetts Institute of Technology, Cambridge, MA 02139, USA

and W. Wade Adams
Wright Laboratory, Materials Directorate, WL/MLPJ, Wright Patterson Air Force Base, OH 45437-7702, USA

Low-voltage, high-resolution scanning electron microscopy (LVHRSEM) is a promising new technique for polymer morphological characterization, and provides complementary data to transmission electron microscopy, X-ray scattering and the scanning probe microscopies. Practically, lateral resolution on the order of 50 Å at 1.0 keV accelerating voltage can be obtained in polymer samples. The utility of LVHRSEM is demonstrated for diverse polymer systems, both amorphous and crystalline, with structurally interesting features on a 50–1000 Å length scale. The advantages and disadvantages of LVHRSEM as a polymer characterization technique are investigated, as well as the effects of beam–sample interactions, radiation damage and contamination specific to polymers examined at low voltage.

(Keywords: low-voltage HRSEM; contrast mechanisms; morphology)

INTRODUCTION

The elucidation of polymer morphology has historically been accomplished using optical microscopy (OM), conventional transmission electron microscopy (TEM), X-ray scattering and, more recently, for crystalline polymers, high-resolution TEM (HRTEM). These techniques have proven to be more useful, and therefore more common, than conventional thermionic-source scanning electron microscopy (SEM) in the realm of polymer characterization due to the readily interpretable nature of the data and, for TEM and X-ray scattering, the higher-resolution information they provide. Although extremely valuable, the two-dimensionality of TEM data and the globally averaged nature of X-ray data have limits when trying to determine the three-dimensional microstructure of materials at small length scales. The direct visualization of three-dimensional specimen structure such as that provided by SEM would be an advantageous complement, provided conventional SEM resolution was greatly improved. Obviously, parallel improvements in sample preparation are also necessary in order to resolve meaningful information within the sample. Conventional SEM has typically been used for lower-resolution (1 μm or greater) applications, such as fracture surfaces and composites, but not to characterize polymer microstructures, where features on the order of 100 Å are often present[1].

Polymer samples are inherently more difficult to image than metals in both the SEM and TEM for many reasons. Most polymers are composed primarily of carbon and hydrogen: the combination of low atomic number and low density results in poor electron scattering, which gives low contrast. Although conducting polymers have recently been synthesized, most polymers are insulators; their non-conducting nature causes both charge and thermal build-up in the sample when bombarded with electrons. The local accumulation of charge and heat can result in dimensional changes due to the loss of sample stability, decomposition and/or crosslinking of the polymer chains. Such effects are particularly noticeable in beam-sensitive samples. Charging necessitates coating samples with a conductive metal film; for conventional SEM, a coating thickness of 100–200 Å is typical. These coatings then obscure any fine topographical features of the sample. Also, polymers may contain contaminants such as residual solvent and low-molecular-weight fractions, which can degas from the sample surface when placed under vacuum. As these contaminants degas at the sample surface and the electron beam collides with these molecules, they can polymerize to form a contamination layer on the sample surface. All of the above phenomena serve to degrade micrograph image quality and prevent the highest resolutions from being attained.

Recent advancements in SEM technology have significantly increased resolution. In particular, these technological improvements have been optimized to allow for SEM operation at low accelerating voltages. Low-voltage SEM (0.5–5.0 keV) of polymers is advantageous over conventional SEM imaging (10–35 keV) due to reduced

* Presented at 'Aspects of Imaging in Polymer Science', 51st Annual Meeting of the Microscopy Society of America, 1–6 August 1993, Cincinnati, OH, USA

† To whom correspondence should be addressed

charging artifacts and significantly improved topographic contrast. The technological improvements include the field emission gun (FEG), a high-excitation, short-focal-length lens and better vacuum. The high-brightness, small-spot-size, low-energy-spread FEG is, perhaps, the most important of these components. This new generation of SEM technology, known as high-resolution SEM (HRSEM), presents a promising technique for polymer morphological characterization. Practically, resolution on the order of 50 Å at 1.0 keV in a polymer sample is attainable. HRSEM should become routine in polymer characterization as a complementary technique to TEM, X-ray scattering and the scanning probe microscopies (scanning probe microscopy (SPM), atomic force microscopy (AFM) and scanning tunnelling microscopy (STM)).

In this paper we address the advantages and disadvantages of low-voltage high-resolution SEM as a characterization technique for polymeric materials. The low-voltage HRSEM (LVHRSEM) images presented here were obtained on a Hitachi S-900 FEG, immersion-lens SEM. We will also discuss the effects of beam–sample interactions, radiation damage, contamination specific to polymers at low voltage and the various operative contrast mechanisms.

CONVENTIONAL VS. LOW-VOLTAGE, HIGH-RESOLUTION SEM

Significant work using SEM to study synthetic polymers began in the late 1960s. For 20 years after these first studies, the smallest features imaged in polymer samples have typically been 1–10 μm. The evolution of the LVHRSEM now provides polymer scientists with the opportunity to topographically image structures on the order of 50–100 Å, a level of microstructure usually investigated with TEM or X-ray scattering. The potential for improved understanding of polymer morphology is significant, especially when LVHRSEM data are combined with information from other techniques. No longer is the polymer community limited to using SEM for low-resolution applications; LVHRSEM can become an important investigative technique in basic polymer physics research. An added advantage associated with all SEM is the ease and speed of sample preparation. The developments that have led to LVHRSEM and the differences between conventional and high-resolution SEM will be outlined in this section.

We define a conventional SEM as a large-chamber microscope with a tungsten-hairpin electron source, a long-focal-length objective lens and moderate vacuum (10^{-6} Torr at the gun and 10^{-5} Torr at the sample). The sample is always placed beneath the objective lens and secondary electrons are collected off to the side of the sample by a scintillator–photomultiplier detector (Everhart–Thornley detector)[2]. At 35 keV, the resolution is typically 50–400 Å; and at low keV, resolution degrades to the order of 500–1000 Å. Conventional SEMs are most often operated between 10 and 35 keV due to limited resolution at lower voltages.

We define a high-resolution SEM as a microscope with a FEG electron source, a short-focal-length objective lens and a relatively high vacuum (10^{-9} Torr at the gun and 10^{-6} Torr at the sample). The sample is placed inside the pole pieces of the objective lens (immersion-lens system), just as in TEM. The secondary electrons generated spiral back up the column and are collected by a detector placed above the upper pole piece of the objective lens (a through-the-lens detector or TTL detector).

Field-emission (FE) SEMs with a different sample/detector configuration are also available; the chamber is large and the sample is placed beneath the objective lens as in conventional SEM. These large-chamber FE SEMs have somewhat lower resolution than the 'high-resolution' immersion-lens systems, with resolutions of 15 Å at 30 keV and 75 Å at 1.0 keV in ideal samples, as compared to resolutions of 6 Å at 30 keV and 35 Å at 1.0 keV in the immersion-lens system.

Most of the technology needed to build a high-resolution SEM has been in existence for a long time, but it was the semiconductor industry's need for low-voltage SEM to reduce radiation damage that provided the impetus for the improvements that have led to the 'high-resolution' SEM[3]. Perhaps the most significant of these technological advances has been the practical stabilization of the field emission gun, which was actually first used in a SEM in 1942[4]. The most common FEG is a dual cold-cathode system with an electron source made of a single-crystal tungsten tip that is etched to a radius of curvature of approximately 1000 Å. The tip is oriented such that the low-work-function (310) crystallographic planes of tungsten emit electrons[5]. The FEG is three orders of magnitude brighter than a tungsten-hairpin source and has an order of magnitude smaller energy spread, both of which factors are especially important when operating at low voltage.

Theoretically, resolution improves with increasing accelerating voltage because the wavelength of electrons decreases and chromatic aberration is significantly reduced with increasing voltage. The lateral resolution is greater than or equal to the diameter of the incident probe and therefore limited by the smallest attainable probe size. The equation for incident probe diameter showing the contributing factors is given by[4]:

$$d_{\text{probe}} = \{(i/B\alpha^2)^2 + (1.22\lambda/\alpha)^2 + [(\Delta E/E)C_c\alpha]^2 + (0.5C_s\alpha^3)^2\} \quad (1)$$

The first term represents the square of the practical electron probe diameter, which is the diameter at which the current density falls to one-fifth the maximum value. The constant B in this term is directly proportional to the brightness of the electron source and i is the beam current. For a FEG the first term becomes very small because the brightness is three orders of magnitude larger than for a tungsten-hairpin source. The second term represents the diffraction limit to probe size and is proportional to the wavelength of the electrons λ, and inversely proportional to the beam divergence angle α. The diffraction limit to probe size is minimized when the wavelength of the electrons is small (higher accelerating voltages) and the aperture sizes are large (large α). The third and fourth terms represent the chromatic and spherical aberration limits to probe size, respectively, and will be discussed in further detail. At low accelerating voltages this equation may not be usable for optimizing microscope design, but it is useful here for illustrating the parameters that affect microscope performance.

Because of the voltage/resolution trade-off, the polymer microscopist is constantly faced with a quandary in conventional SEM: either operate at high keV to

maintain resolution and heavily coat samples to eliminate charging, or operate at low keV to reduce charging and sacrifice the resolution capabilities of the microscope. The solution is to image at low keV using a field-emission, immersion-lens microscope, which greatly reduces the effects of chromatic aberration at low voltage via a small-energy-spread beam and a lens with a small chromatic aberration coefficient.

The resolution limit d_c for chromatic aberration is given by[4]:

$$d_c = (\Delta E/E) C_c \alpha \quad (2)$$

where ΔE is the energy spread of the beam, E is the accelerating voltage and C_c is the chromatic aberration coefficient. For a tungsten-hairpin source ΔE is 2–3 eV, whereas for a FEG ΔE is 0.2–0.3 eV. Therefore at high accelerating voltages the effects of chromatic aberration are often insignificant. At low voltages $\Delta E/E$ can be quite large, so the energy spread ΔE needs to be minimized, which is accomplished with the FEG. Also the chromatic aberration coefficient is 2–3 mm in the short-focal-length immersion-lens system, as compared to approximately 10 mm for the long-focal-length lens in the large-chamber SEM[4,5]. The FEG also produces a very small spot size, on the order of a few nanometres, and requires little or no demagnification, whereas the tungsten filament requires large demagnifications to produce a spot size of tens of nanometres in diameter.

The immersion lens system offers several other advantages over the conventional SEM arrangement such as lenses optimized for use at low voltage and a smaller spherical aberration coefficient. The resolution limit d_s for spherical aberration is given by[4]:

$$d_s = 0.5 C_s \alpha^3 \quad (3)$$

where C_s is the spherical aberration coefficient. The spherical aberration coefficient is approximately 2 mm in the short-focal-length immersion-lens system, as compared to 20 mm for the long-focal-length lens in the large-chamber SEM[4,5].

On the other hand, the immersion-lens system also presents the biggest disadvantages to employing HRSEM: (i) a limitation in sample size and (ii) a very small depth of field. Samples can be no larger than a few millimetres on a side and approximately 3 mm high. In a large-chamber SEM the depth of field can be increased by imaging at longer working distances, although at the same time resolution is compromised. The depth of field D in a large-chamber SEM is given by[4]:

$$D = 2r/\alpha \quad (4a)$$

$$\alpha = R/WD \quad (4b)$$

where r is the radius of the beam at the point where the beam overlaps two picture elements and is inversely proportional to the magnification, α is the beam divergence angle, as given above, R is the radius of the final aperture and WD is the working distance. The depth of field can be varied by changing the final aperture, working distance or magnification in a large-chamber SEM. In an immersion-lens system the depth of field is fixed for a given magnification.

All things considered, it is the level of detail or the smallest microstructural length scale in a material that will determine the ultimate advantage of high-resolution SEM over conventional SEM. Obviously, the smaller the polymer feature being investigated, the more advantageous LVHRSEM becomes. We have investigated a wide variety of polymer systems, both amorphous and crystalline, with the LVHRSEM and compared image quality and resolution to data obtained by conventional SEM. *Figure 1* shows comparison images of the uncoated liquid-nitrogen tensile fracture surface of a mesophase pitch-based P-25 carbon fibre. The images in *Figures 1a* and *1b* were taken on a JEOL 840 tungsten-filament conventional SEM at 5.0 keV, whereas the images in *Figures 1c–e* were taken on a Hitachi S-900 FEG immersion-lens SEM operated at 2.0 keV. The differences in the level of detail are apparent, even in the low-magnification images (*1a* and *1c*). *Figure 1c* and the out-of-focus upper portion of *Figure 1d* demonstrate the depth-of-field limitations in the immersion-lens microscope. For rough fracture surfaces such as these in the carbon fibres, the limited depth of field in the immersion-lens system often makes it difficult to obtain images at low magnification with the whole image in focus, whereas in the conventional SEM images of *Figures 1a* and *1b* the whole image is in focus. *Figure 1e* is a high-magnification image of the core region of the fibre and clearly presents a level of microstructural detail not apparent in the conventional SEM images. The individual, curved sheet-like structures of mesophase pitch-based carbon fibre are clearly visible[6]. This image was originally taken at 100 000×, whereas 'empty' magnification was reached in the conventional SEM at 25 000×. Empty magnification is the maximum magnification at which an image provides useful information and is dependent upon both the resolution of the microscope and the microstructural length scales present in a sample.

BEAM–SAMPLE INTERACTIONS

The bombardment of a material with high-energy electrons results in several sample–beam interactions. Among these are the production of characteristic X-rays, bremsstrahlung, elastically scattered primary electrons known as 'backscattered' electrons and inelastically scattered 'secondary' electrons produced by the interaction of the primary or backscattered electrons with the valence-shell electrons of the material. The backscattered electrons are defined as having an energy greater than 50 eV up to the energy of the primary electrons, whereas the secondary electrons are defined as having an energy of less than 50 eV. The secondary electron escape depth for insulating organic materials is approximately 200 Å and remains approximately constant with voltage[7]. By comparison, metal conductors have a secondary electron escape depth on the order of 50 Å. In this paper we will be primarily focused on the production and collection of secondary electrons.

A schematic of the beam–sample interaction showing backscattered and secondary electrons in a large-chamber SEM is shown in *Figure 2*[8–10]. Backscattered and secondary electrons produced within a few nanometres of the point of impact of the primary beam are known as BSE_I and SE_I, respectively[11]. Scattering of the primary beam can also result in the production of backscattered electrons at various distances from the point of impact of the primary beam (BSE_{II}). These backscattered electrons

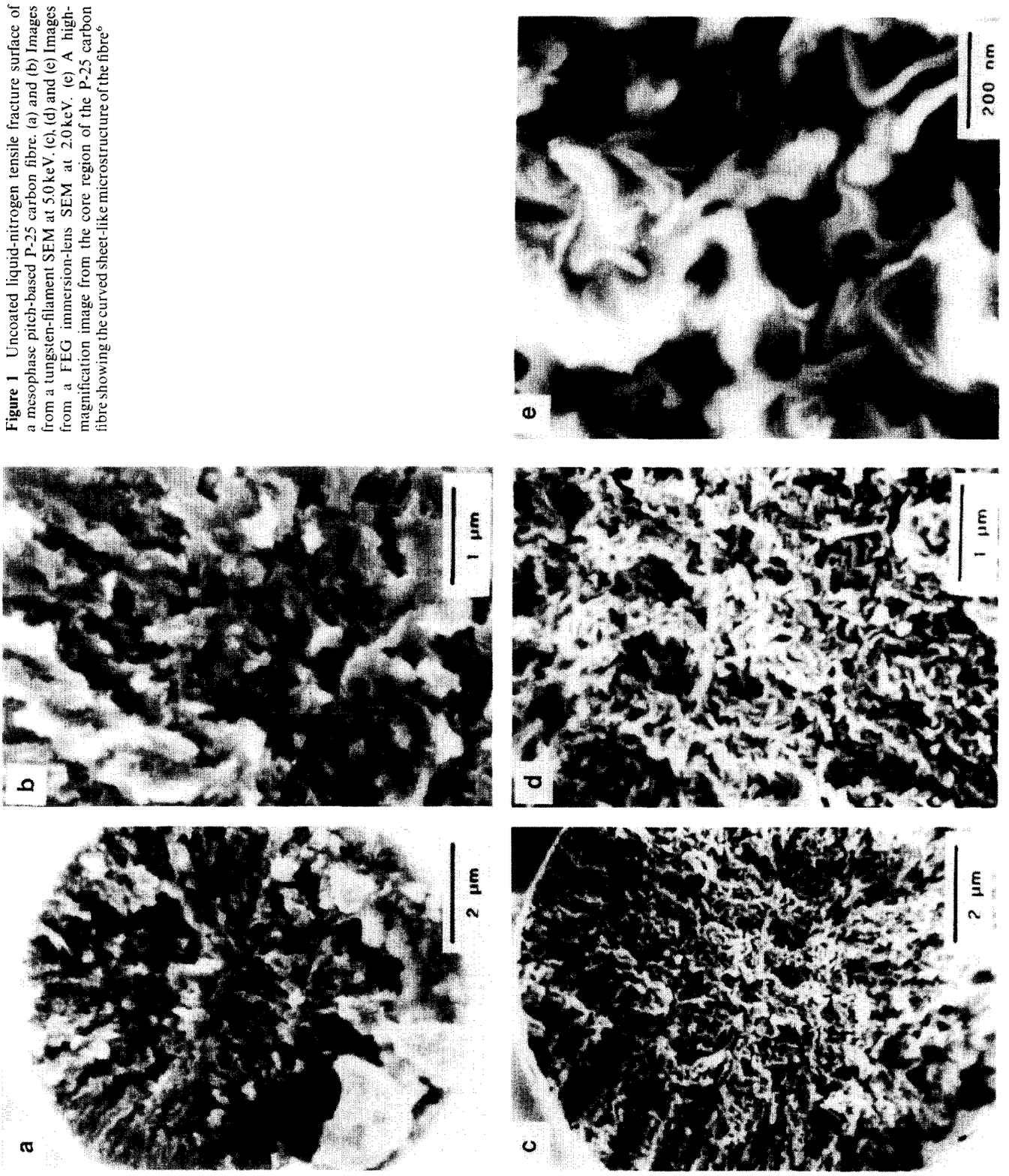

Figure 1 Uncoated liquid-nitrogen tensile fracture surface of a mesophase pitch-based P-25 carbon fibre. (a) and (b) Images from a tungsten-filament SEM at 5.0 keV. (c), (d) and (e) Images from a FEG immersion-lens SEM at 2.0 keV. (e) A high-magnification image from the core region of the P-25 carbon fibre showing the curved sheet-like microstructure of the fibre[6]

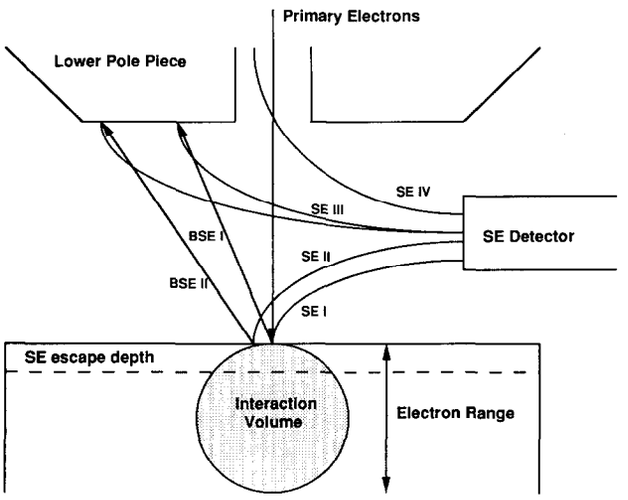

Figure 2 Schematic of the beam–sample interactions in a large-chamber SEM. At low voltage the SE_I and SE_{II} components provide high-resolution information, whereas the SE_{III} and SE_{IV} components are noise, which degrades the signal-to-noise ratio

then produce secondary electrons (SE_{II}) at various distances from the point of impact of the primary beam. After the backscattered electrons exit the sample, they can collide with, for example, the lower pole piece of the objective lens and generate additional secondary electrons (SE_{III}). Secondary electrons can also originate in the upper part of the column and spiral down with the primary beam (SE_{IV}). The SE_I signal provides the high-resolution topographical information from the sample. SE_{II} gives lower-resolution information, while the SE_{III} and SE_{IV} are a noise component in the signal. The SE_I component is usually 20–30% of the total secondary electron signal, and the combined SE_{III} and SE_{IV} component can be as high as 60%[9,10]. The immersion-lens system virtually eliminates the SE_{III} and SE_{IV} components due to the placement of the secondary electron detector above the objective lens, thereby significantly increasing the signal-to-noise ratio.

High-resolution imaging

The SE_{II} distribution is approximately the same size as the SE_I distribution at low voltage because the electron range (the maximum distance the electrons travel within a sample) is several orders of magnitude smaller than at high voltage. Topographic contrast is maximized when the number of secondary electrons produced within the secondary electron escape depth is maximized; for a given number of electrons into a sample, the electron density and therefore the number of scattering events per volume is higher the smaller the range. Because secondary electrons by definition have low energy, they can only escape from the near-surface region of the sample. The greater the electron scattering intensity near the surface, as with a small electron range at low voltage, the greater the secondary electron emission coefficient δ, and the more secondary electrons that are emitted from the surface. The secondary electron coefficient is a measure of the number of secondary electrons produced per incident primary electron. At low keV, δ can be greater than or equal to unity, depending upon the material. Maximum secondary yield occurs when the electron range is approximately two times the secondary electron escape depth, which for most polymers corresponds to an electron range of approximately 400–500 Å. It is therefore desirable to decrease the electron range to approximately 500 Å, which in turn maximizes the secondary electron coefficient, and for low accelerating voltages maximizes the number of high-resolution secondary electrons emitted from the sample.

The SE_I and SE_{II} components have voltage-dependent emission distributions centred about the point of impact of the primary beam, as shown in *Figure 3*[11]. The SE_{II} component has a wider distribution than the SE_I component, which is known as beam tailing. Beam tailing is a function of atomic number, density and voltage. At high voltage, the SE_{II} beam tail can be several *micrometres* across, considerably degrading resolution. Alternatively, at low accelerating voltages the SE_{II} distribution is only slightly larger than the SE_I distribution. Therefore the SE_{II} component is effectively providing the same level of resolution information as the SE_I component in the image. Low-atomic-number, low-density polymer samples have a larger beam tail at all voltages than metals. Thus there are two methods by which high-resolution information can be obtained: operate at high voltage with a raster (the area over which the beam is scanned) small enough so that the SE_{II} contribution is a flat background signal, or operate at low voltage where the SE_{II} beam tail is small. Operation at high accelerating voltages will increase the resolution attainable in the microscope, but it also produces a very large beam tail. At low magnifications the area scanned is larger than the dimensions of the beam tail, and the beam tail (SE_{II} component) then varies and contributes significantly to the image, which degrades resolution in the image. The solution then for attaining high resolution at high voltage is to take images at very high magnification so that the area scanned contains a relatively flat portion of the beam tail. The second method for obtaining high-resolution images is to operate at low voltage where the

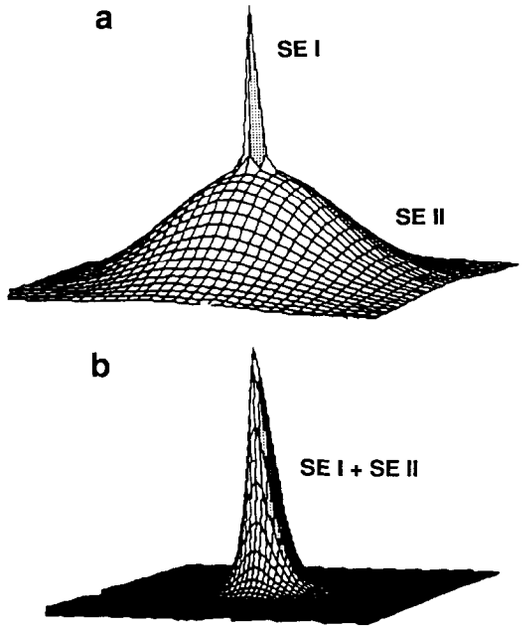

Figure 3 Relative SE_I and SE_{II} emission distributions: (a) high voltage; (b) low voltage. Reprinted with permission from ref. 11

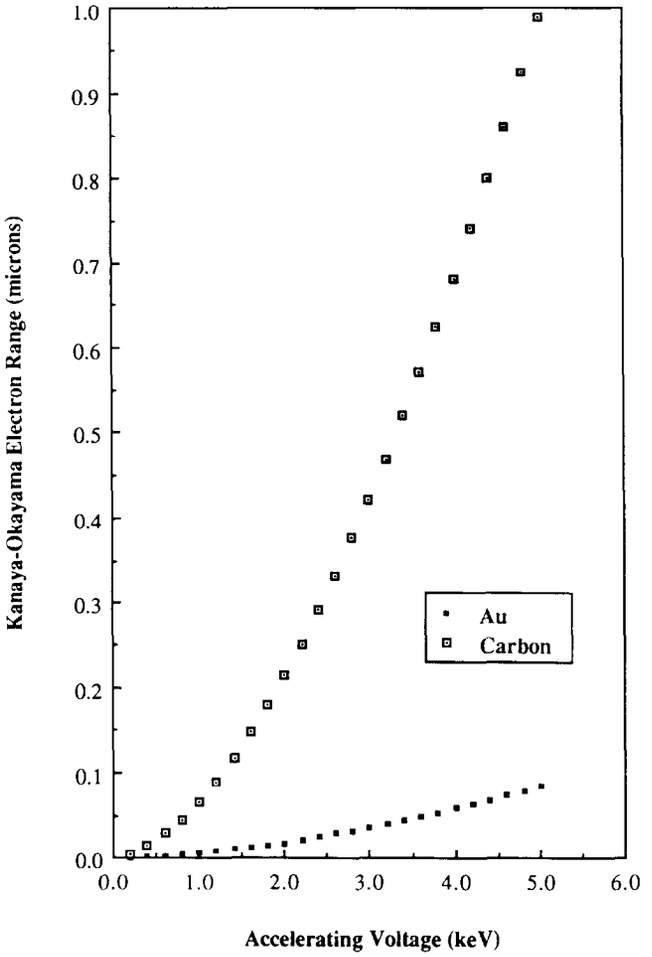

Figure 4 Plot of Kanaya–Okayama electron range vs. accelerating voltage from 0 to 5.0 keV for gold and carbon

beam tail is small and the SE_{II} signal is effectively an SE_I signal, which improves the signal-to-noise ratio because more high-resolution secondary electrons are produced. The overall microscope resolution is slightly compromised by operating at low voltage, but good resolution at all magnifications is then available as well as improved topographic contrast in polymeric materials. Low-voltage operation is the preferred method for polymers; not only is the signal-to-noise ratio improved as more high-resolution secondary electrons are produced, but sample charging is minimized.

Electron range

There are many ways to calculate the electron range. A simple empirical method of Kanaya and Okayama gives the range in micrometres as[4,12]:

$$R_{KO} = 0.0276 A E_0^{1.67} / (Z^{0.889} \rho) \quad (5)$$

where R_{KO} is the Kanaya–Okayama electron range (μm), A is the atomic weight (g mol^{-1}), E_0 is the accelerating voltage (keV), Z is the number-average atomic number and ρ is the density (g cm^{-3}) of the sample. This empirical equation has been found to closely approximate experimentally determined ranges. As can be seen from the equation, the range increases with increasing accelerating voltage, decreasing atomic number and decreasing density. The minimum range is obtained by low-voltage imaging of a dense material with high atomic number.

Figure 4 is a plot of electron range vs. accelerating voltage from 0 to 5.0 keV for gold and carbon (assumed $\rho = 1.0$ g cm^{-3}). For a given accelerating voltage, the electron range for gold is an order of magnitude smaller than for carbon. Specific values are summarized in *Table 1*. Note that for carbon at 1.0 keV the range is 670 Å and at 10 keV approximately 3 μm. *Figure 5* shows 400 Å thick lamellae, edge-on, in a polyethylene blown film coated with 40 Å Cr, imaged at 800 eV, 1.0 keV, 2.0 keV and 5.0 keV. The 800 eV and 1.0 keV images are of the same area and the 2.0 keV and 5.0 keV images are of the same area. These images demonstrate the beneficial effect of reduced electron range on topographic contrast. The 1.0 keV image has better topographic contrast than the 800 eV image, presumably because the resolution limit of the microscope has been reached at 800 eV, as this is the minimum attainable voltage for this particular microscope. The topographic contrast appears more flat in the 2.0 keV and 5.0 keV images as the interaction volume gets larger. The 'flattening' of a polymer surface imaged at high voltage and the resulting loss of structural detail is the biggest problem in conventional SEM ($\geq$ 10 keV) aside from charging. The uppermost surface structure of some polymers can even appear translucent with the loss of fine detail when imaged at high voltage, because the backscattered electrons generated deep within the sample produce secondary electrons as they exit the surface.

Crossover

The total number of electrons exiting a material divided by the number of incident primary electrons is defined as the electron yield. The electron yield varies as a function of accelerating voltage and has the form shown in *Figure 6*. An electron yield of 1.0 occurs at two places on this plot. These points are termed the crossover voltages, with the lower-voltage crossover designated E_1 and the higher-voltage crossover designated E_2. E_2 for most insulators ranges from 500 eV to 3.5 keV. E_1 is usually too small to measure with existing LVHRSEM technology. The section of the curve between E_1 and E_2 defines the voltage range where positive charging occurs, in which more electrons are exiting the sample than entering, resulting in a net charge depletion at the surface. When imaging, positive charging manifests itself as a darkened region in the sample, as the net positive field locally retards the electron yield. The section of the curve at voltages greater than E_2 with an electron yield less

Table 1 Kanaya–Okayama electron range as a function of voltage

Accelerating voltage (keV)	Range (Å)	
	Carbon	Gold
0.8	460	40
1.0	670	60
2.0	2140	180
3.0	4220	360
4.0	6820	590
5.0	9990	850
10.0	31500	2700
15.0	62000	5300
20.0	100000	8600
25.0	145500	12500
30.0	197300	17000

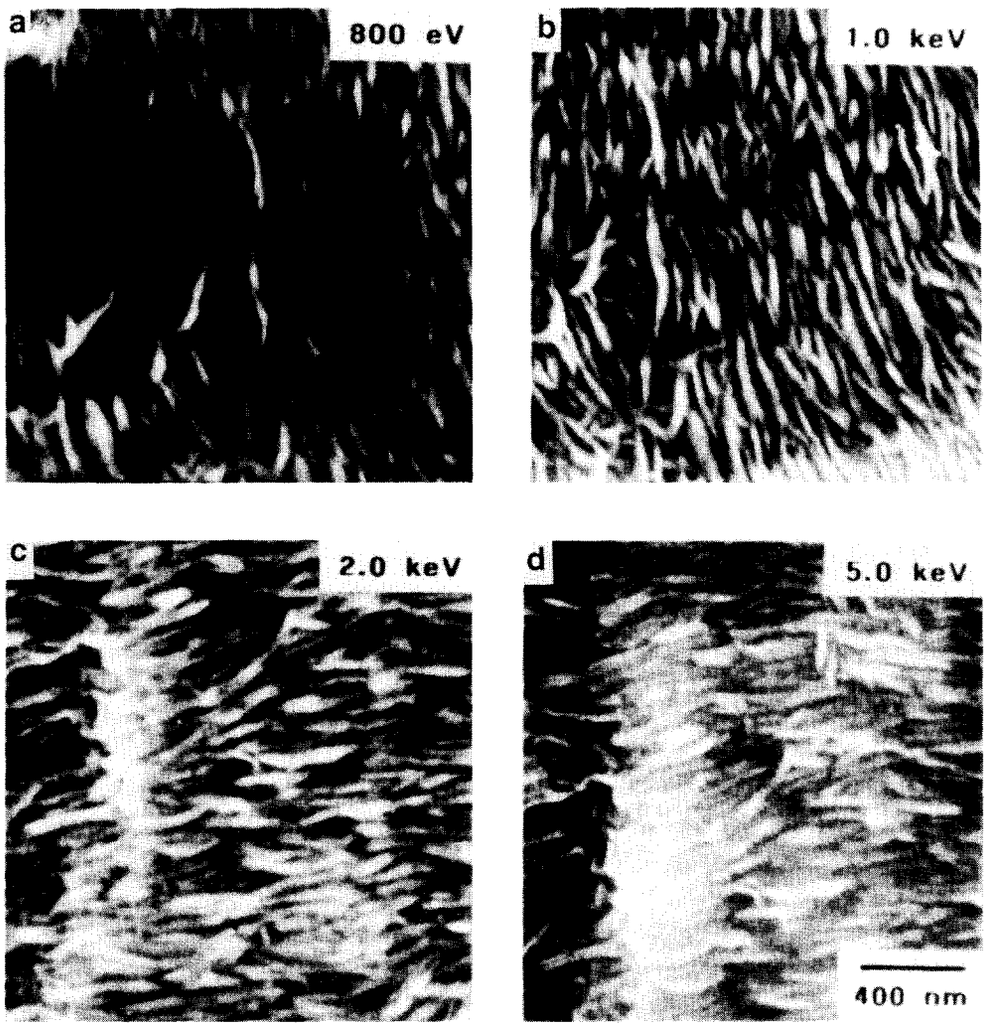

Figure 5 LVHRSEM images of 400 Å thick lamellae in a polyethylene blown film coated with 40 Å of chromium and imaged at (a) 800 eV, (b) 1.0 keV, (c) 2.0 keV and (d) 5.0 keV. The surface topographic contrast flattens as the accelerating voltage increases. Figure pairs (a) and (b) are of the same area as are (c) and (d)

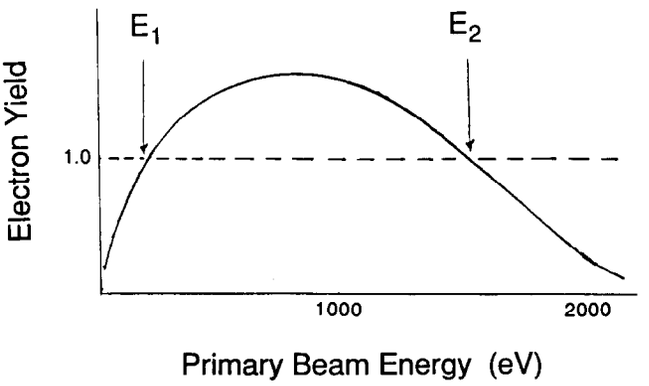

Figure 6 Total electron yield vs. accelerating voltage showing the E_1 and E_2 crossover voltages at which the electron yield equals 1.0

than 1.0 is known as the negatively charged region, in which fewer electrons are exiting the sample than entering. Negative charging results in a charge build-up within an insulating, uncoated sample and manifests itself as very bright regions. Negative charging can produce fields large enough to deflect the incident electron beam away from the sample or even back up the microscope column. Ideally, to eliminate charging in an insulating sample, an acceleration voltage equal to E_2 should be used.

There have been several reports of both calculated and experimentally determined E_2 crossovers for polymers[13,14]. Theoretically, a crossover voltage can be calculated for a given material but practically the crossover depends on what microscope is used, how the sample is mounted (grounding conditions), scan speed, magnification, condenser lens current, the surface roughness, surface contamination and alterations in the specimen structure as a function of electron dose (radiation damage). The crossover can also be shifted by tilting the sample. There can be localized regions of both positive and negative charging in a given sample as shown, for example, in the uncoated, 100 Å thick polyethylene single crystals deposited on carbon-coated mica in *Figure 7*. The dark, multiple overgrowth regions charge positively whereas the bright monolayer regions in contact with the substrate charge negatively at an accelerating voltage of 1.0 keV.

Charging patterns can be changed by varying the substrate and/or accelerating voltage. *Figure 8* is an image

Figure 7 LVHRSEM image of localized positive and negative charging in uncoated polyethylene single crystals on carbon-coated mica at 1.0 keV

of polyethylene single crystals on carbon-coated mica taken at 800 eV, rather than at 1.0 keV as in *Figure 7*. The sample does not discharge as it did at 1.0 keV, and stable imaging is achieved. The individual polyethylene monolayers are about 100 Å thick. At 800 eV the majority of the scattering events with respect to the first monolayer are taking place within the substrate due to the fact that the electron range for carbon at 800 eV is approximately 450 Å. The substrate is therefore contributing significantly to the bright contrast in the first monolayer. As the thickness of the sample increases (number of overgrowth layers increases), the substrate contributes less to the image contrast. The contrast changes from bright for the first layer, to grey for the second layer, to black for the third layer, and back to grey for all other successive layers. This variation in contrast with thickness is due to the change in crossover for each layer (up to the fourth layer) because of the variation in the substrate contribution to the image. The contrast mechanism operative in the first three layers is a 'thin-film' contrast, because the electron range is greater than the thickness of the polymer film. In the fourth layer and all successive layers, a 'bulk' contrast mechanism is present, as it is only the contrast generated from the electron-beam interactions with the polyethylene (no substrate) that produce contrast. Variations in contrast arise from surface topography and the resulting increase in secondary electron emission at the layer edges, which are discussed in the next section.

Tilting effects and surface topography

Topographic contrast arises when there are local differences in the efficiency at which the secondary electrons are collected or local differences in the secondary electron coefficient (local variations in crossover). Except for metals examined at low keV, local differences in the secondary electron coefficient arise wherever there is an edge or a local tilting of the surface with respect to the primary beam direction, as in the case of surface roughness. At an edge, secondary electrons can escape from the top surface as well as the side surface as shown in *Figure 9a*, as a greater percentage of the interaction volume is within the secondary electron escape depth. Tilting also increases the secondary electron yield by moving the interaction volume closer to the surface. The secondary electron coefficient is increased with tilt, as shown by the equation:

$$\delta(\theta) = \delta_0 \sec\theta \tag{6}$$

where δ_0 is the secondary electron coefficient at a normal angle of incidence and θ is the tilt angle. Tilting is therefore an effective way of reducing charging in a polymer sample examined at a voltage greater than E_2 by shifting the crossover to higher voltages as shown by Vaz with poly(tetrafluoroethylene) (PTFE or Teflon), acetal and poly(vinyl chloride) (PVC)[15]. *Table 2* summarizes Vaz's measured crossovers for these uncoated materials at 0° and 60° tilt in a JEOL 840 tungsten-hairpin filament microscope at 1.0 nA beam current. The

Figure 8 LVHRSEM image of a portion near the edge of an uncoated, multiple-overgrowth, large polyethylene single crystal, imaged at 800 eV on carbon-coated mica. The contrast variation is due to the change in crossover for each layer because of the variation in substrate contribution to the image

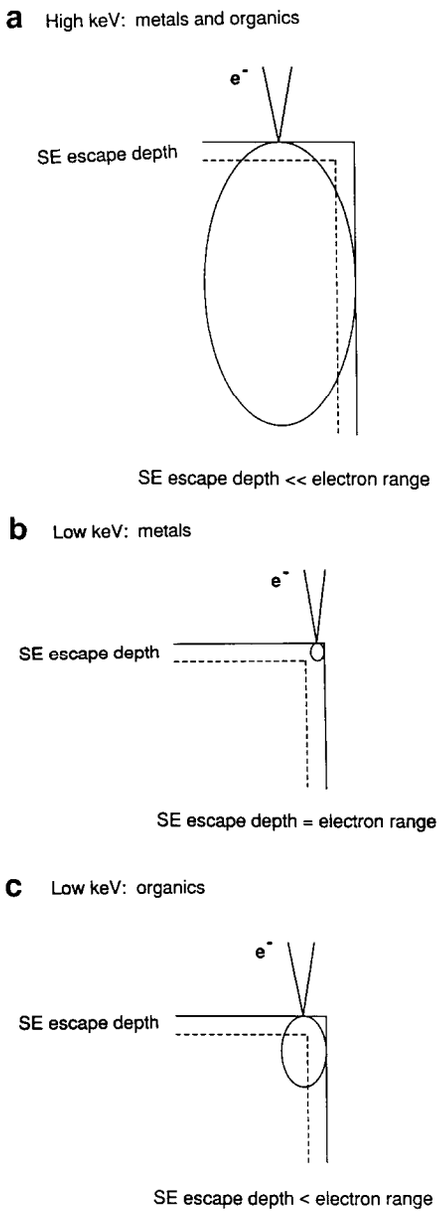

Figure 9 Tilting and edge effects as a function of material and voltage. (a) At high voltage, both metal and polymers have increased secondary electron emission when the sample is tilted and at edges. (b) At low voltage, contrast in metal samples decreases because the electron range is approximately the same as the secondary electron escape depth. (c) At low voltage, contrast in polymer samples improves because the electron range is small, but still larger than the secondary electron escape depth

measured crossover voltages for these polymers roughly double upon tilting by 60°, which is due to the fact that the calculated secondary electron coefficient doubles when the sample is tilted by 60° (equation (6)). He also found that slower scan speeds and higher magnifications (higher current densities) shift the measured crossovers to lower voltages.

In metals at low accelerating voltage, the electron range is approximately the same distance as the secondary electron escape depth. For example, in gold at 1.0 keV the electron range and the secondary electron escape depth are approximately 50 Å. The result is a *loss* of edge contrast because the electron range is within the secondary electron escape depth at every place on the sample. Therefore tilting results in no change in the secondary electron coefficient and no change in contrast. A schematic of this effect is shown in *Figure 9b*.

In polymers, however, topographic contrast is present and even enhanced at low keV operation. Even at low accelerating voltages the interaction volume in a polymer is always much larger than the roughly 200 Å secondary electron escape depth. Therefore, topographic contrast has the same origins as at high voltage. At low voltages the topographic contrast is enhanced, as discussed previously, because the total interaction volume is smaller and closer to the surface. A schematic of this effect is shown in *Figure 9c*.

Differences in collection efficiency can arise when the detector is placed off to one side of a rough sample as in large-chamber microscopes. Those topographic features which face towards the detector appear brighter as more secondary electrons emanating from their surfaces are collected. This difference in collection efficiency produces a (sometimes beneficial) shadowing effect in the image.

COATED VS. UNCOATED SAMPLES

Charging in polymers necessitates coating samples with a conductive metal film in conventional SEM imaging. Thick coatings of gold, gold–palladium or platinum–palladium, typically 100–200 Å thick, are either evaporated or sputtered onto the sample. Carbon is sometimes also used. The coatings are thicker than the secondary electron escape depth for metals at low voltage, which means that the secondary electron signal collected actually arises only from the coating material, not from the polymer sample itself. These thick coatings also obscure any fine topography present in the sample—the situation is somewhat analogous to taking a picture of a landscape after a heavy snowfall. One can only infer what is underneath a thick coating, be it metal on a polymer or a blanket of snow on the landscape. The longer times required to deposit thick coatings and the resulting heat build-up in the sample can also alter the microstructure present[16].

Low-voltage operation reduces or eliminates the need for coating. Most often charging is only reduced, not eliminated, because, even when operating at the supposed crossover voltage for a given polymer, local variations in the crossover still usually occur, for reasons discussed previously. Often samples can be imaged uncoated at TV rates on the CRT, but a photo cannot be collected because the slower scan rates necessary to record the image increase charging. A framegrabber, which is a device that takes the digital output of the CRT and integrates the data over a predetermined and variable number of rastered images, is often useful in obtaining photos at fast scan speeds. If a framegrabber is available, images of uncoated specimens can be collected directly; if not, samples must be coated. Even when a framegrabber is

Table 2 Measured crossover voltage as a function of tilt in a JEOL 840 tungsten-hairpin filament microscope at 1.0 nA beam current[15]

	Crossover (keV)	
Polymer	0° tilt	60° tilt
Poly(tetrafluoroethylene)	1.9	3.5
Acetal	1.7	3.1
Poly(vinyl chloride)	1.7	3.5

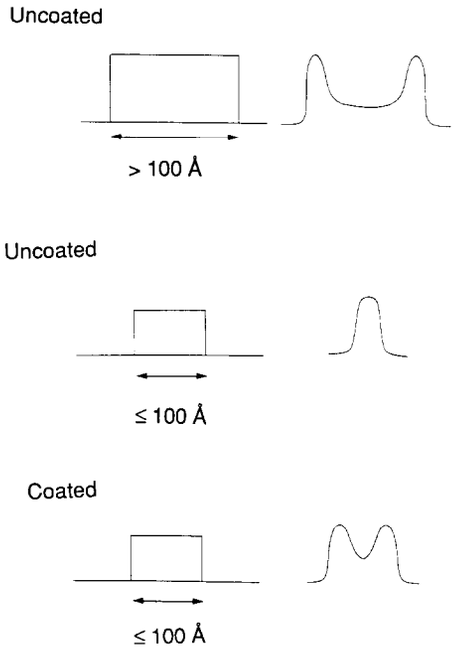

Figure 10 Schematic of the secondary electron line profiles for particles of different dimensions. Uncoated particles less than 100 Å in size result in one peak, whereas coated particles less than 100 Å in size result in two peaks. Reprinted with permission from ref. 11

available, charging often occurs in uncoated samples at reduced raster when focusing and stigmating the image, especially at high magnification. Practically, and for ease of operation at low keV, many polymer samples must still be coated.

New coating technologies such as dual ion-beam sputter coaters now allow for extremely thin continuous conductive coatings to be applied[17]. Typically tungsten or chromium is used as the coating material, as these materials can produce a 10 Å thick conductive film. The grain sizes for 10 Å coatings are small enough not to be discernible at magnifications greater than 100 000×. When samples are coated with a thick conducting film as with conventional SEM, the samples can be imaged after weeks or months without any charging problems. This is not the case when a 10 Å thick metal film is used. Metals have a much higher surface energy than polymers (100–1000 vs. 30–60 dyn cm^{-1}), and as a result the metal coating will diffuse into the polymer sample with time. This diffusional behaviour of the metal was directly observed by Schwark[18] in TEM images of cross-sectional microtomed sections of styrene–butadiene block copolymers that had a surface coated with gold. The gold atoms preferentially diffused into and reformed grains at a depth of approximately 2000 Å within the butadiene layers. Our experience has shown that, once most polymers are coated with a 10 Å layer of tungsten, they must be imaged the same day, or they must be re-coated just before imaging, because samples will charge when attempting to image later.

At this time, most polymer microscopists do not have access to the new (and expensive, approximately US$50 000) dual ion-beam coaters that are capable of producing 10 Å thick continuous films, However, for low-voltage imaging conventional thick coatings should *not* be used in the HRSEM because high-resolution images of the metal grains are obtained rather than the desired images of the polymer surface. A solution to this technological limitation is to sputter-coat samples with gold–palladium for a short amount of time (roughly 15 s) with an inexpensive sputter coater in the normal operating manner of the device[19]. Then image the sample, and if charging persists, repeat the procedure. The procedure can be repeated until charging is eliminated. We have used this method quite effectively without large metal grains forming on our samples.

The continued need to coat polymer samples is not necesssarily a negative aspect in LVHRSEM. Even when there is no need to coat a sample, it may be advantageous to apply a 10 Å coating to improve the surface feature resolution. According to Joy, the classical limit to spatial resolution in organic materials is 50–200 Å, or approximately the mean free path of secondary electrons for a given material[11]. This limit can be overcome by coating the polymer surface with a 10 Å metal film, which has a mean free electron path of approximately 50 Å vs. 200 Å for a polymer. *Figure 10* is a schematic of the secondary electron line profiles for particles of different dimensions. Uncoated particles less than 100 Å in size result in one peak in the profile, whereas particles larger than 100 Å show two peaks, one at each edge of the particle. After coating, particles smaller than 100 Å will give rise to two peaks because the thin metal coating increases the secondary yield by attenuating the overall electron range, which keeps the interaction volume closer to the surface. This method of coating small polymeric features with thin metal films may also aid in determining particle shape.

RADIATION DAMAGE

Radiation damage to polymers is of major concern in both TEM and SEM, since in both cases high-energy electron beams impinge upon organic samples. A high-energy electron interacts strongly with a given polymer, the interaction being dependent upon such factors as beam energy, sample temperature, sample composition, sample structure (e.g. crystalline vs. amorphous, orientation, stresses present within the sample), thickness and type of conductive coating, and residual gases in the microscope column. There are many possible types of radiation damage that can occur. The incident electron deposits energy in a cascade of events, which generate molecular fragments, secondary electrons and X-rays, as well as sample heating. In addition to primary events (radical and fragment formation) caused by the probe, secondary chemical changes (crosslinking, unsaturation, evolution of gases and molecules) can take place at a rate dependent on the concentration of the respective species and the specimen temperature (which influences molecular and radical mobility)[20–22]. Differences in the coefficients of thermal expansion between the metal coating and the polymer may also result in cracking of the sample upon heating by the beam.

Since the various aspects of radiation damage usually result in disordering of the polymer sample (e.g. crosslinking, mass loss), radiation damage effects in crystalline materials are more easily characterized[23]. Such effects also take place in amorphous polymers, but it is difficult to monitor them quantitatively. In TEM of crystalline polymers, radiation damage is manifested by the destruc-

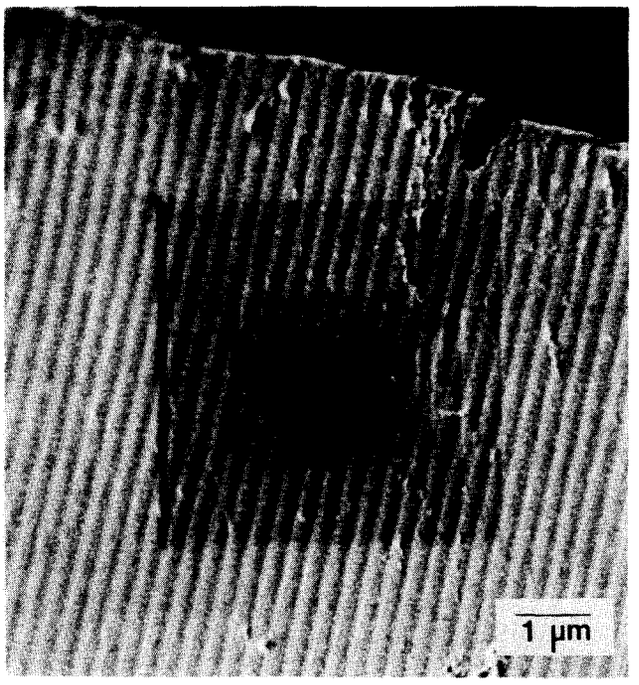

Figure 11 Mass loss from a 1.0 keV beam in an amorphous polyacrylate polymer dispersed liquid-crystal film. The liquid crystal has been removed. Mass loss is visible as the darkened area in the shape of the raster

tion of long-range order within the sample. The diffraction contrast fades from bright-field and dark-field images in concert with the loss of Bragg peaks in reciprocal space[24]. Mass loss is easily detected in bright-field images by an increase in transmitted beam intensity. Crystalline polymeric materials imaged in the SEM usually have prominent features related to their crystalline order such as lamellae, spherulites, or microfibrils. The loss of long-range order in the crystalline lattice is not detectable via SEM but dimensional changes from the normal anisotropy of an irradiated film or chain-folded lamellae can cause large dimensional changes resulting in surface warping[25,26]. For example, an oriented polyoxymethylene sheet undergoes beam-induced cracking from a combination of chain scission and the residual stresses resulting from thermoprocessing[27]. Except for mass loss, radiation damage in amorphous polymers is difficult to detect, but the primary beam–sample interaction is unchanged and independent of whether the polymer is ordered. *Figure 11* is an example of SEM beam-induced mass loss in an amorphous polyacrylate polymer dispersed liquid-crystal holographic film imaged at 1.0 keV. The polyacrylate has been photopolymerized in the form of a Bragg diffraction grating, which causes the blended small-molecule liquid crystal to phase-separate into neighbouring lamellae (visible as channels in the image)[28,29]. In this sample the liquid crystal has been removed with methanol. The mass loss is visible as the dark regions that are in the shape of the raster.

In SEM imaging it is usually thought that radiation damage decreases as accelerating voltage is decreased, because experimentally less surface cracking, etc., is observed in samples at lower operating voltages. However, because the energy deposited by the incident beam varies with depth, the deposited energy density increases with depth up to the range R of the electron. Although the total deposited energy per electron is smaller at low keV, the deposited energy is significantly more localized than for a higher-energy beam. There have been no quantitative studies on the radiation damage effects of low keV electron beams on polymers, so it is still unknown whether more or less radiation damage occurs at low voltage.

A useful strategy to determine if beam damage is occurring in a given specimen in the SEM is to examine the specimen under minimum-dose conditions and record a series of images as a function of total incident beam dose. The procedure is to use a TV scan rate to locate a feature of interest at low magnification. Then, at high magnification, focus and stigmate the image, although these operations may cause radiation damage, charging of the sample and contamination. One then translates the beam, using the image shift controls, to an adjacent area, which has only received a very low dose during the TV rate viewing at low magnification. If available, the use of a framegrabber to integrate fast (TV rate) multiple scan images allows for some dissipation of heat and charge. When radiation damage is a problem, the magnification should be selected such that features of interest are just resolved, yielding the lowest electron dose possible for the desired information. A series of images can then be acquired and the development of any beam-induced specimen structure can be monitored, thus avoiding the interpretation of any artifacts as 'real' structure within the sample.

CONTAMINATION

Contamination on the surface of a polymer is of major concern in SEM as it is the information from the surface texture of the polymer that is of interest. Surface contamination has the same effect as coating a sample; fine topography is obscured or its shape modified, resulting in artifacts within images. The improved vacuum technology built into the HRSEM has greatly reduced contamination originating from within the microscope system. It is obvious, but frequently disregarded, that specimen preparation for surface analysis must avoid introduction of various impurities such as finger grease and salts on the sample surface. Assuming adequate sample preparation, the major source of contamination when imaging polymers is the polymer sample itself. Polymeric samples are frequently 'dirty' when compared to other materials; any residual solvent, plasticizers, low-molecular-weight fractions present in the polymer, or fragments caused by electron beam-induced scission are likely to degas through the surface. The electron beam may then polymerize these hydrocarbons, resulting in the build-up of a contamination layer on the surface.

Often when an image in the HRSEM is taken at low voltage, a darkened area in the shape of the raster appears on the sample surface. This darkened area results from the previous high-magnification adjustment of focus/stigmation and may arise from beam damage, contamination and/or positive charging. It can be difficult to distinguish the relative contributions of each of the mechanisms that are active. This darkened area may be the result of the polymerized hydrocarbon contamination

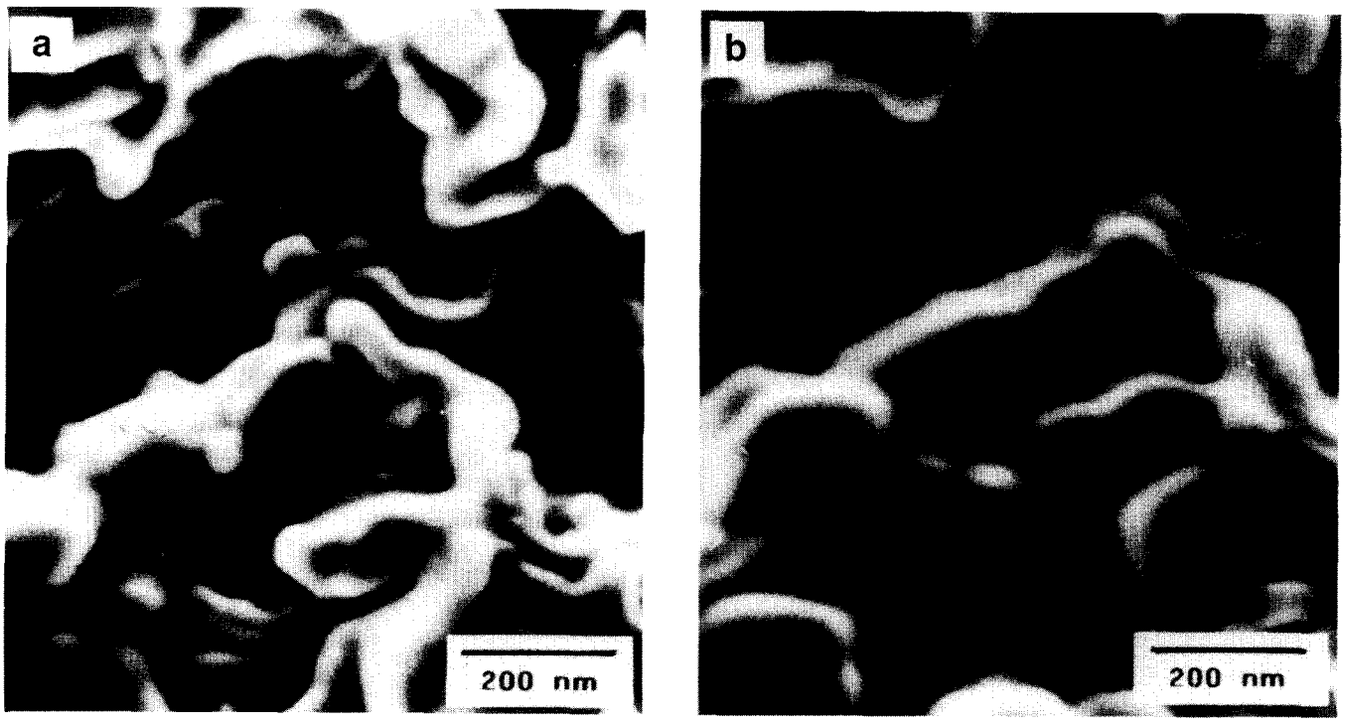

Figure 12 LVHRSEM stereopair images of contamination on a P-25 carbon fibre fracture surface. Image (a) was taken prior to (b). The curved, sheet-like structures are obscured when compared to the image in *Figure 1e*

layer discussed above, which, because it is an insulator, often positively charges, enhancing the darkened contrast. The darkened region does not necessarily arise from the presence of a contamination layer, but may be due solely to positive charging of the sample in the highly irradiated area.

Contamination occurs at both high- and low-voltage operation, but is more visible in low-voltage imaging, as proportionately more signal is generated and collected from the contamination layer at low keV than high keV. Therefore, in order to derive optimum information from the sample, great care must be taken to reduce surface contamination when performing LVHRSEM of polymers. A cold finger should always be employed to cryo-pump microscope column gases, whereby adsorbed molecules may be degassed from the specimen. Alternatively, residual solvent, plasticizers and low-molecular-weight fractions can be immobilized by the use of a sample cold stage. In some instances a sample hot stage may be used to reduce contamination in thermally stable polymers. However, due to the physical nature of many polymers, with their low melting points and glass transition temperatures, a cold stage is preferable for most applications. *Figures 12a* and *12b* are examples of the effects of contamination on image quality. Shown are stereopairs of a P-25 carbon fibre fracture surface, similar to the one shown in *Figure 1e*. The contamination was due to the undesired and inadvertent presence of pump oil in the microscope column. *Figure 12b* was taken after *12a* with the increase in contamination evident in the image. The normal curved sheet-like structures have been obscured and no longer resemble the actual microstructure present in the sample as shown in *Figure 1e*.

CONSTRAST MECHANISMS

There are several possible contrast mechanisms that can be present when imaging a polymer surface at low keV. Each mechanism can act singularly or in conjunction with another contrast mechanism. The contrast mechanisms discussed below are all the result of the detection of secondary electrons, although the production of secondary electrons can be affected by factors such as surface topography, the backscattered electron coefficient (sample composition), crossover effects, beam/sample geometry, sample conductivity and, for thin polymers such as single crystals, the substrate can play a large role in the observed contrast. Image interpretation is not always a straightforward process, and great care must be taken to understand the effects of microscope configuration as well as the contribution of each contrast mechanism to the final image. The various mechanisms we have encountered in our samples will be discussed in the following sections.

Topographic contrast

In LVHRSEM, topographic contrast is the primary means of obtaining information about a polymer surface. Topographic contrast arises from variations in the local secondary electron yield produced at edges and from surface roughness and is also greatly affected by the position of the detector relative to the sample. If the detector is directly above the sample the contrast in the image will appear the same for each feature upon rotation of the sample about a vertical axis (beam axis). Most often in conventional SEM, the secondary electron detector is placed off to the side of the sample and the

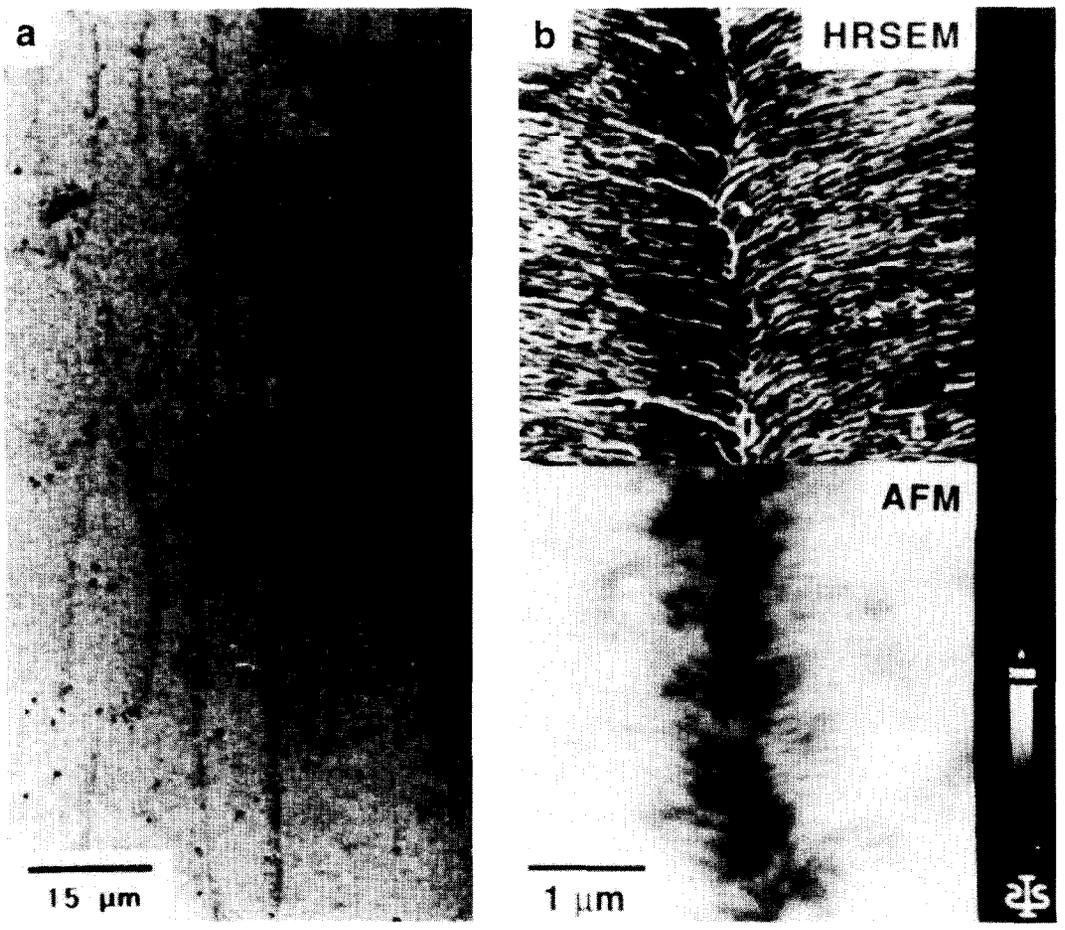

Figure 13 Thermotropic nematic liquid-crystalline polyester aligned in a magnetic field. Sample has been quenched, annealed and etched to produce surface relief topography. (a) Low-magnification LVHRSEM image showing the inversion wall loop with dark contrast. (b) Composite high-magnification LVHRSEM/AFM images of the inversion wall. The wall is three-dimensional with the centre of the wall being deeper than the edges

contrast in the image is due to differences in collection efficiency for each feature. A shadowing effect is then present in the image. Rotation of the sample results in contrast changes for each feature. The microscopist must therefore always be aware of the detector position relative to features in the sample for proper interpretation of images.

In the Hitachi S-900 immersion-lens SEM, operation at low voltage requires that the detector be placed to one side of the sample (to reduce or eliminate the influence of the detector field on the incident beam) as well as above the upper pole piece of the objective lens. A shadowing effect is therefore present[30], but another effect of detector placement has been observed: higher features of the surface topography appear brighter, presumably due to differences in collection efficiency. As the secondary electrons from the sample spiral back up the column to the detector, those generated in higher regions have a greater collection efficiency than those from lower regions.

Figure 13a is a low-magnification HRSEM image of a thermotropic liquid-crystalline polyester taken at 1.0 keV. The polymer was aligned in a magnetic field, quenched, annealed and etched with methylamine as described in detail elsewhere[31]. The dark loop is an inversion wall defect in which the molecules on one side of the wall are rotated 180° with respect to the molecules on the other side of the wall. At low magnification the loop appears darker than the surrounding polymer because there is a valley at the centre of the inversion wall defect, which has been confirmed by atomic force microscopy and is shown in the lower portion of *Figure 13b*. Also note that the left side of the image is brighter than the right side, presumably because the detector is above and to the left of the sample in this microscope. We have also observed this height-dependent contrast in stereopairs of carbon fibre fracture surfaces, where height differences are large, even over small areas. The three-dimensional structure of the inversion wall is shown in the composite LVHRSEM/AFM image in *Figure 13b*. The upper portion is a higher-magnification LVHRSEM image of the inversion wall. Pure topographic contrast can be seen in the lamellae where the edges are brighter than the centre of the lamellae due to local changes in the secondary electron yield. The lower portion is an AFM height image (repulsive mode), showing that the inversion wall valley is approximately 2000 Å deep.

What is the height resolution or minimum peak-to-valley distance parallel to the beam that can be detected in the HRSEM? The lateral resolution of the HRSEM at 1.0 keV in polymers is roughly 50 Å, but the height resolution is at present unknown. The height resolution

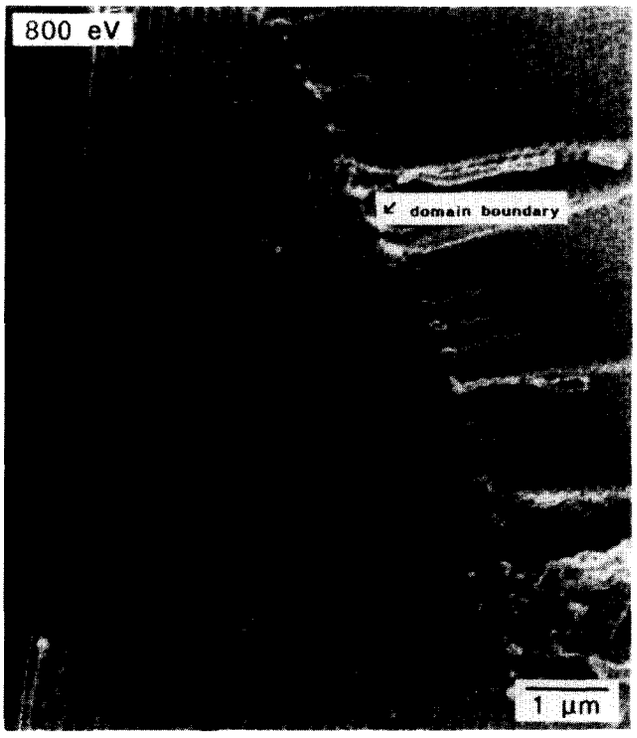

Figure 14 LVHRSEM image of a room-temperature fracture surface of a glassy siloxane cholesteric liquid-crystal macromolecule. The periodicity in the image corresponds to one-half the pitch of the cholesteric

should be a function of many parameters including the secondary electron coefficient of the sample at the voltage used, crossover, operating voltage, height profile (sharpness of the edge) and coating. If the observed structure has a periodic texture, such as the siloxane cholesteric liquid crystals and the lamellar block copolymers discussed below, the spatial frequency of the features will also affect the resolution observed by the naked eye. Intermediate spatial frequencies are visible at much lower contrast than either high or low spatial frequencies[32]. The height resolution will also depend upon whether bulk or thin-film contrast is present as in the polyethylene single crystals in *Figure 8*. Thin-film contrast, which is much stronger than the bulk, edge contrast in the polyethylene single crystals, may allow one to probe very small changes in height.

Figure 14 is a LVHRSEM image of the *fracture* surface of a glassy (at room temperature) siloxane cholesteric liquid crystal taken at 1.0 keV[33]. The fracture surface is corrugated with a periodicity of 1800 Å, which corresponds to one-half the pitch of the cholesteric. AFM has shown that the peak-to-valley distance is 150–200 Å. We tried to image a *free* surface of these materials with LVHRSEM, but the surface appeared featureless. However, upon observation by AFM and cross-sectional TEM the corrugation with a periodicity of 1800 Å was again observed with a peak-to-valley height of only 25–50 Å. The limit to height resolution for *this sample* at 1.0 keV is therefore somewhere between 50 and 150 Å.

Figure 15 is a LVHRSEM image of an unstained polystyrene–polybutadiene (40 000–40 000 molecular weight) lamellar diblock copolymer free surface with the lamellae approximately perpendicular to the surface. Cross-sectional TEM and AFM have shown that this surface is not flat, but corrugated with the periodicity of the lamellae (600 Å lamellar repeat)[34]. The polybutadiene lamellae correspond to the peaks in the corrugation and the polystyrene lamellae to the valleys. The peak-to-valley height measured by AFM is 60–120 Å. The observed contrast in these LVHRSEM images is a combination of both topographic contrast due to the corrugated surface and presumably compositional contrast due to the compositional difference in the alternating lamellae. The compositional difference enhances the topographic contrast, so the height resolution due strictly to topographic effects cannot be determined with this sample. It should be noted that the contrast in the polystyrene–polybutadiene diblock copolymer could be significantly enhanced by staining the butadiene domains with OsO_4, a process that preferentially increases the average atomic number and density of the polybutadiene domains as shown in *Figure 16a*. *Figure 16b* shows the effect of a 40° tilt on contrast in this sample. The contrast decreases because the interaction volume contains regions from both types of compositional domains. The contrast is averaged based on the percentage of each domain in the local interaction volume.

Compositional contrast

Compositional contrast arises from variations in electron emission based on atomic number Z. At high accelerating voltages (≥ 15 keV) compositional contrast is detected by the collection of backscattered electrons. The backscattered electron coefficient η increases monotonically with increasing Z, whereas the secondary electron coefficient δ varies much less predictably with Z. At low keV the backscattered yield is very low;

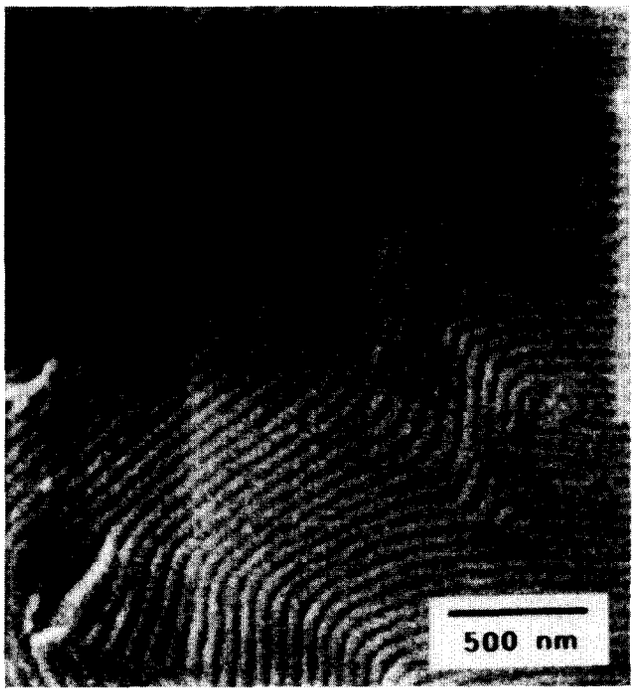

Figure 15 LVHRSEM image of unstained polystyrene–polybutadiene lamellar diblock copolymer free surface with lamellae approximately perpendicular to the surface. Contrast is both topographical and compositional in origin

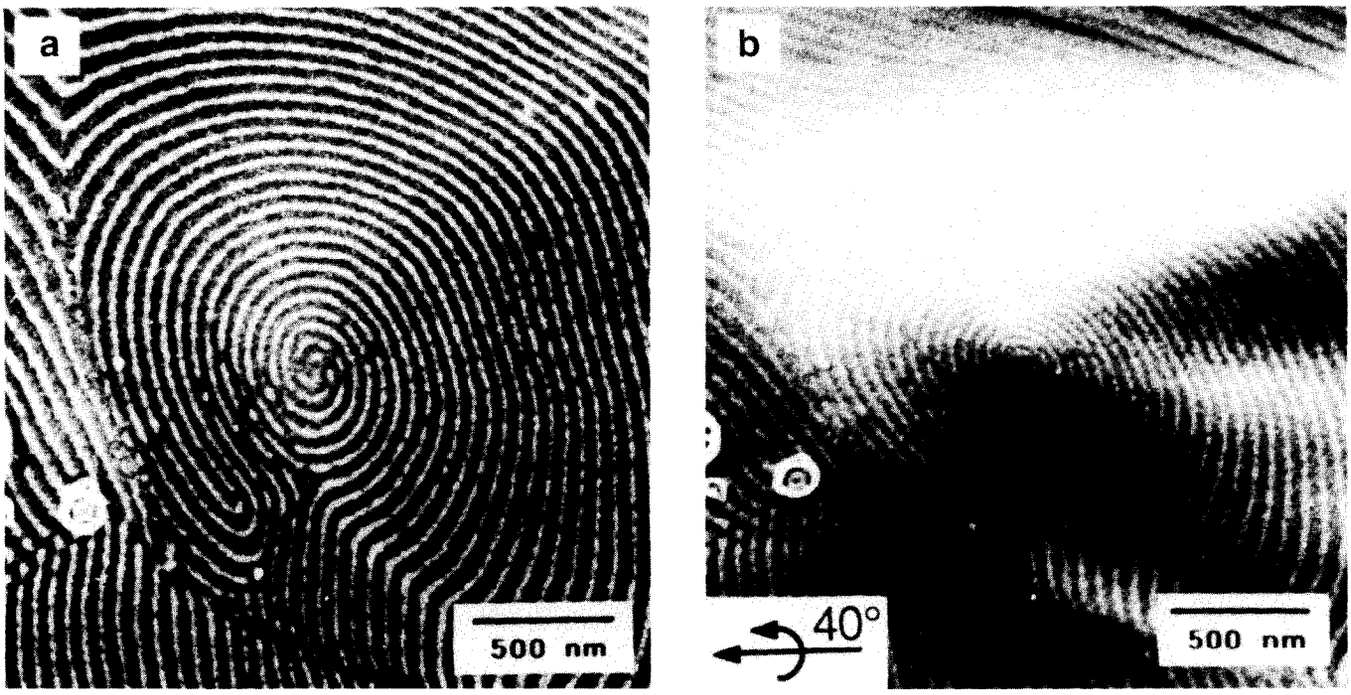

Figure 16 LVHRSEM images of OsO_4-stained polystyrene–polybutadiene lamellar diblock copolymer free surface with lamellae approximately perpendicular to the surface. (a) Beam is perpendicular to the surface and the contrast is greatly enhanced when compared to *Figure 15*. (b) Sample is titled 40 with a resulting decrease in contrast

backscattered imaging is typically done at high keV. Until recently, backscattered detection at low voltage was technologically limited. There are now available microchannel plate detectors for low-voltage operation with good resolution in large-chamber SEMs, but the resolution currently attainable in detectors designed for immersion-lens systems is not at the level of secondary imaging, so backscattered imaging will not be discussed further.

Compositional contrast can play an important role in SEM images at low voltage, as discussed above. Any enhancement of the topographic contrast is a bonus, for the higher the feature contrast the better the resolution. Berry has taken advantage of the combined topographic and compositional contrast present at low voltage and successfully imaged many polymer blends, both stained and unstained, with conventional SEM (LaB_6 source, large chamber) between 0.5 and 1.5 keV at high tilt (to reduce charging, as discussed previously) and small working distance[35]. His samples were microtomed stubs with relatively large domains; microtomed blends have some topography resulting from the uncontrolled fast fracture of a material with components that have different moduli. Therefore, even though microtomed samples are usually thought to be locally flat, there is always topographical contrast in conjunction with the compositional contrast when doing secondary electron imaging.

Compositional modifications can lead to conductivity differences, which result in crossover changes as shown in the ion-implanted poly(*p*-phenylene benzobisoxazole) (PBO) fibre in *Figure 17*[36]. The fibre was implanted with Xe^+ at 100 keV and a fluence of 10^{16} ions cm^{-2}. Ion implantation leads to chemical changes in polymers much like pyrolysis; atoms other than carbon are ejected, crosslinking results and the density increases, leading to an increase in conductivity, although ion implantation is a surface technique rather than a bulk technique like pyrolysis. The near-surface regions of the implanted fibres are conductive and do not charge at 1.0 keV, whereas the unimplanted non-conductive PBO has a crossover voltage below 800 eV and therefore must be coated for imaging. The fibre in *Figure 17a* has been bent; the deformation has caused the implanted skin region of the fibre to crack. The thickness of this implanted layer is about 2000 Å, in good agreement with the theoretically calculated range of Xe^+ in PBO at this energy. Those regions of the skin that are completely separated from neighbouring skin appear darker, as shown in the higher-magnification image in *Figure 17b*, because the most conductive pathway through the skin has been broken and these pieces of skin must now conduct charge away only through the non-conductive, unimplanted PBO core. *Figure 17c* is an image of a surface fractured at liquid-nitrogen temperature. The implanted skin region is much brighter than the unimplanted core because it is more conductive. The horizontal streaking is due to charging of the core region, as this sample was not coated. These figures illustrate how the grounding condition and composition of a material can affect observed contrast.

The substrate can significantly affect the image contrast if the thickness of the polymer specimen is smaller than the electron range at the operating voltage used (thin-film contrast as discussed with respect to *Figure 8*). Substrate effects on contrast are considered compositional effects because it is the crossover of the substrate (which is dependent upon its composition) that can determine the overall contrast in the image. Such is the case for 100 Å thick polyethylene single crystals deposited on various substrates. Because monolayers of these polyethylene crystals are so thin, most of the interaction volume (even

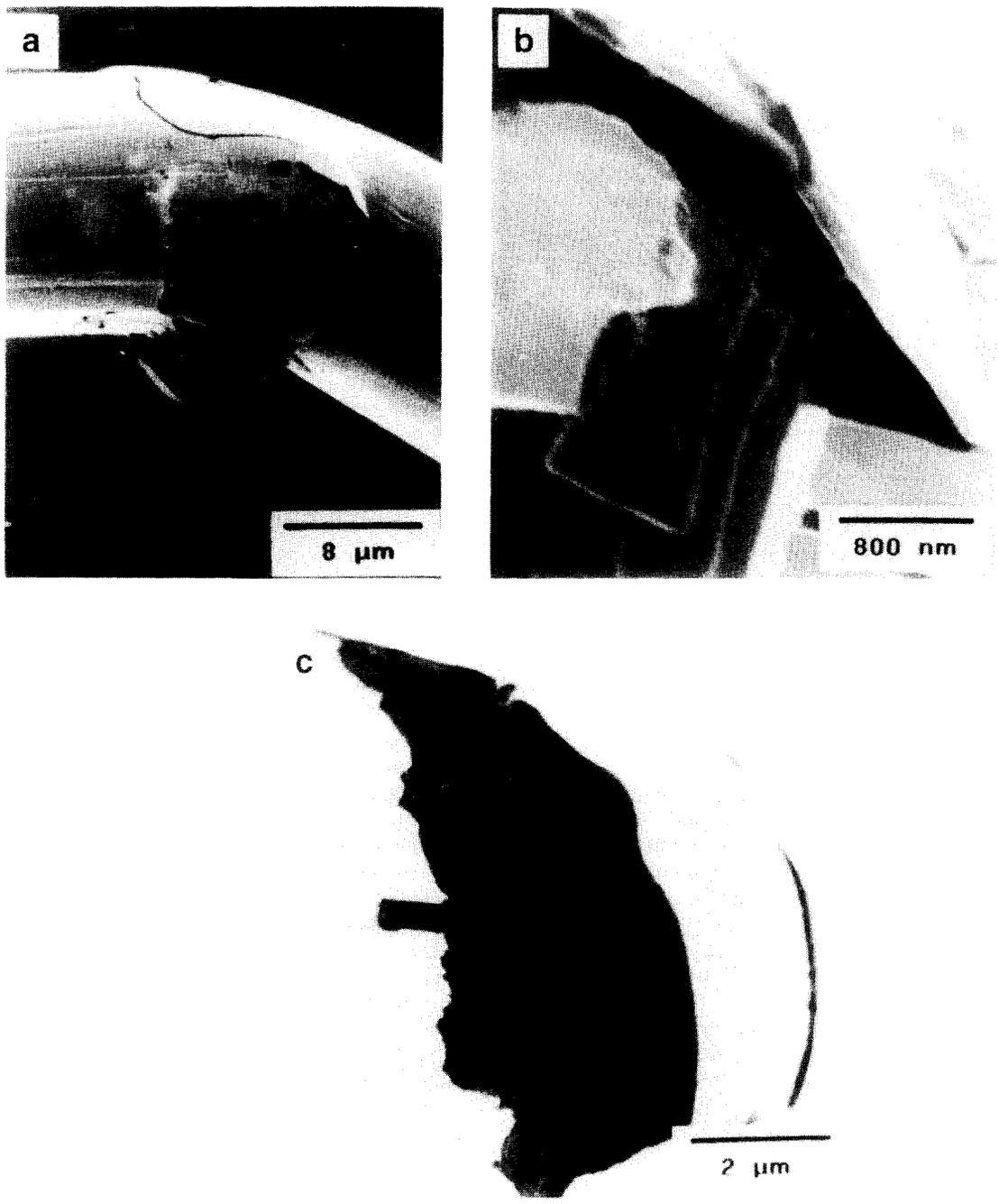

Figure 17 LVHRSEM images of PBO fibre ion-implanted with xenon at 100 keV, 10^{16} ions cm^{-2} fluence. (a) Low-magnification image of a bent fibre. (b) Higher-magnification image of (a). Contrast variations in the implanted skin are observed due to different conductive pathways. (c) Liquid-nitrogen fracture surface showing contrast variation in the implanted skin vs. the unimplanted core

at 800 eV) is contained within the substrate. Thus a large portion of the SE signal originates from the substrate. As voltage is increased, even more scattering events take place within the substrate and eventually the substrate contrast completely dominates the image. Presumably the contrast also depends upon how effectively these tent-shaped crystals collapse and come into electrical contact with the substrate upon deposition. *Figure 18* shows the contrast changes in polyethylene single crystals on an aluminium foil substrate as voltage is systematically varied from 800 eV to 5.0 keV. The polymer monolayers are dark as compared to the bright contrast of the monolayers when deposited on carbon-coated mica in *Figures 7* and *8*. As the voltage increases, the contrast between the crystals and substrate decreases. When two crystals overlap to form a double layer, this double layer is darker than the single layers, as was observed with the crystals on carbon-coated mica. The contrast between the single and double layers decreases as voltage is increased. At higher magnifications, the features of crystals deposited on aluminium foil were more difficult to see than when placed on carbon-coated mica. At all voltages, features of the aluminium foil could be observed through the thin crystals. Very flat substrates are

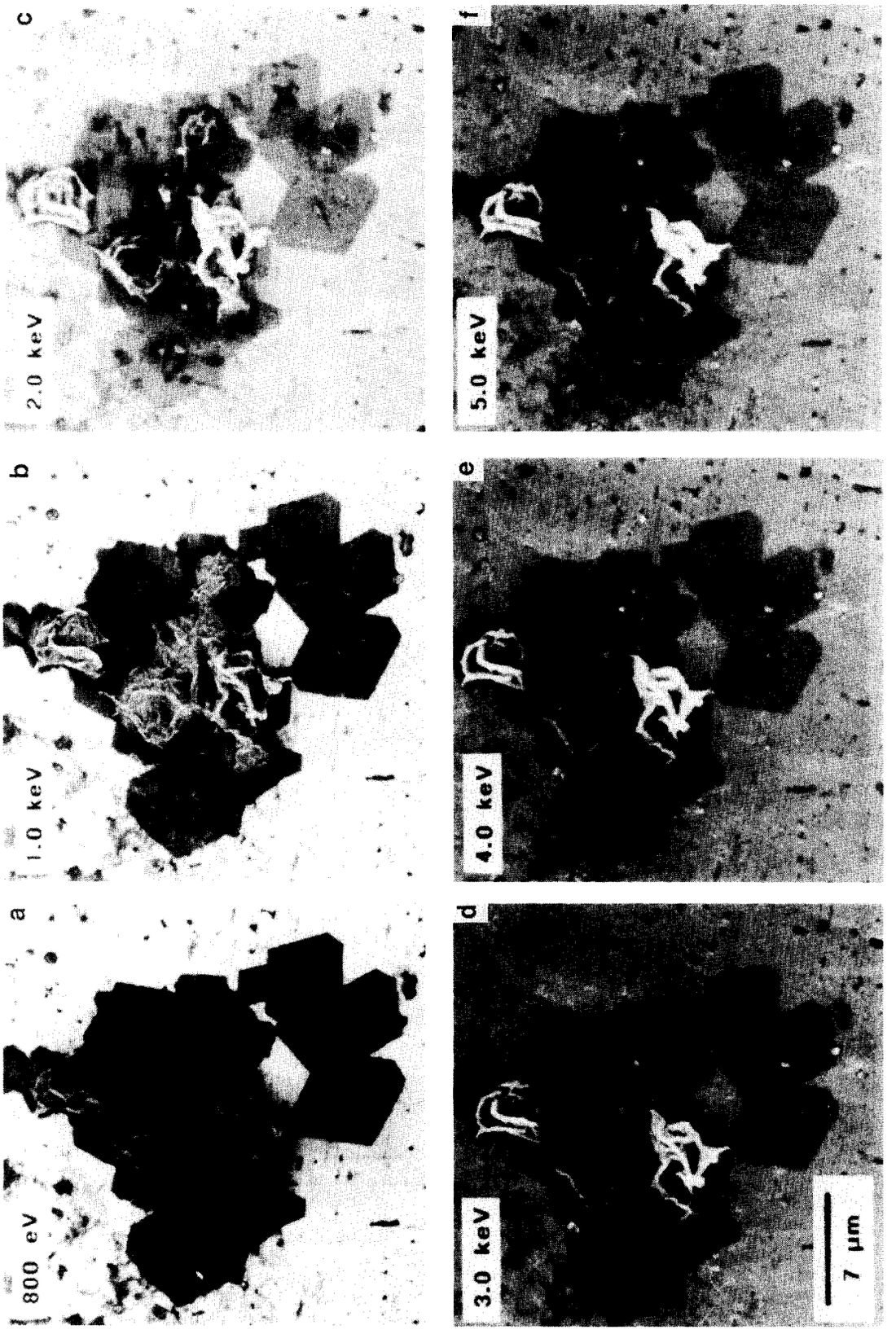

Figure 18 LVHRSEM images of the contrast variation as a function of operating voltage from (a) 800 eV to (f) 5.0 keV for polyethylene single crystals on an aluminium foil substrate

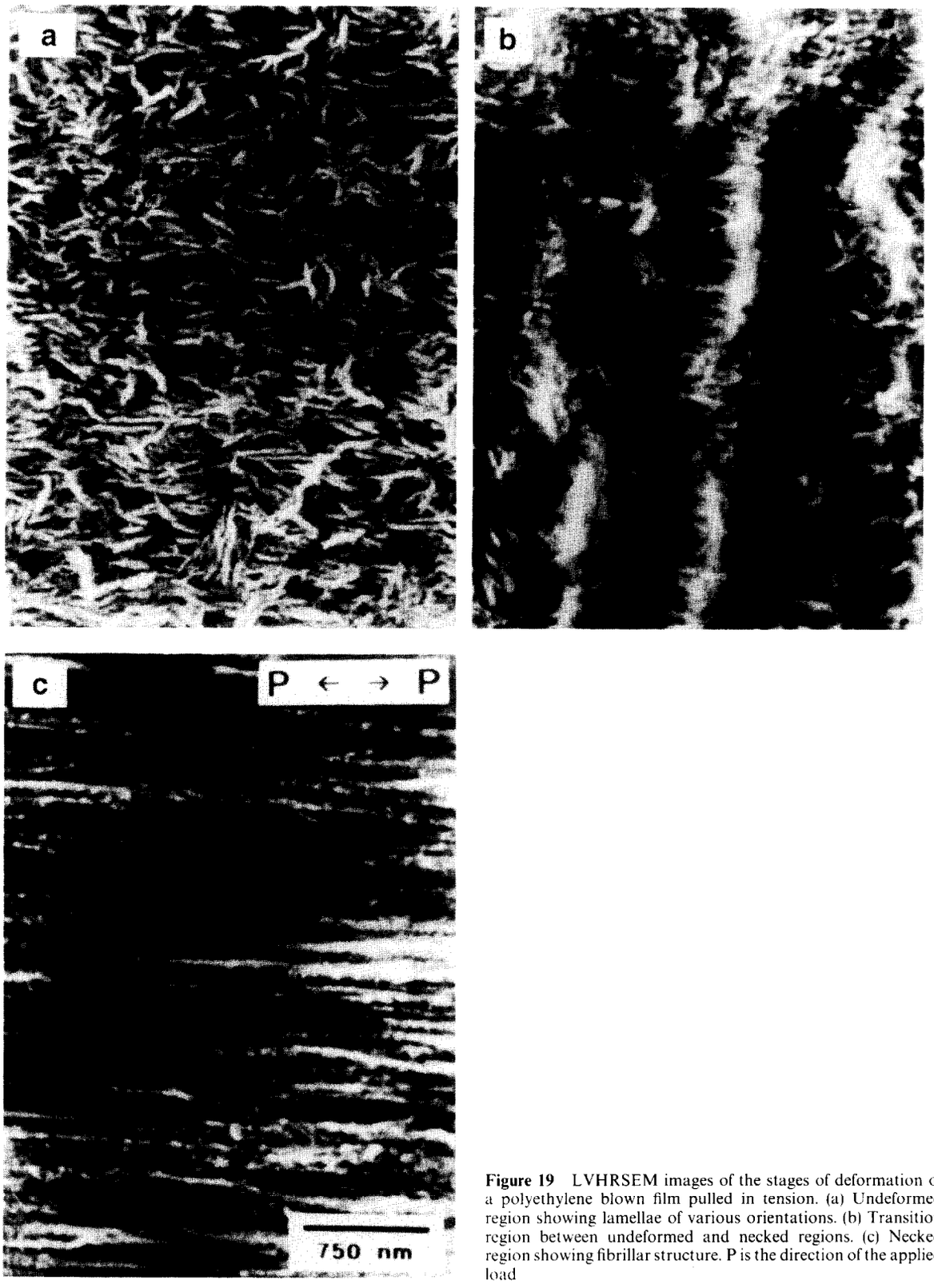

Figure 19 LVHRSEM images of the stages of deformation of a polyethylene blown film pulled in tension. (a) Undeformed region showing lamellae of various orientations. (b) Transition region between undeformed and necked regions. (c) Necked region showing fibrillar structure. P is the direction of the applied load

therefore desirable, and care must be taken when selecting a substrate for observation of polymer thin films.

POLYMER DEFORMATION IN THE HRSEM

In situ deformation of polymers in an immersion-lens SEM at low voltage requires the same type of deformation stage currently available for TEM. For example, the microstructural changes in polyethylene upon deformation have been thoroughly investigated by TEM (bright-field, dark-field and electron diffraction)[37,38], by conventional SEM[39] and by scanning transmission electron microscopy (STEM)[40]. The LVHRSEM can provide complementary information on the changes in

the surface structure of polyethylene upon deformation. *Figure 19* is a deformation series from a section of a polyethylene blown film that has been pulled in tension until necking occurred (*ex situ*). *Figure 19a* is an image from the undeformed region showing 400 Å thick lamellae of various orientation. *Figure 19b* is from the transition region and *Figure 19c* is from the necked region. The lamellae have been drawn out to form fibrillar structures in the necked region. With the proper deformation stage, this experiment could have been performed *in situ* with no coating. However, interpretation of *in situ* deformation images must consider radiation damage, including cumulative crosslinking and mass loss.

CONCLUSIONS

Low-voltage, high-resolution SEM is a promising new technique for polymer morphological characterization. LVHRSEM is a valuable complementary technique to TEM, X-ray diffraction and the scanning probe microscopies in the study of polymer morphology and polymer structure–property relationships. The investigation of polymers by SEM is no longer limited to relatively low-resolution applications. The LVHRSEM can provide microstructural information useful to basic polymer physics research. Recent high-resolution technology allows for operation at low voltage with a practical resolution of 50 Å, and the low-voltage operation reduces or eliminates charging problems common to uncoated polymers. High-resolution ion-beam coaters that can deposit a continuous 10 Å metal coating and reduce coating artifacts are also now available.

The usefulness of LVHRSEM has been demonstrated for diverse polymer systems, both amorphous and crystalline, with structurally interesting features on a 50–1000 Å length scale. The potential rewards of LVHRSEM are great, but a thorough understanding of this technique is necessary to prepare samples properly, optimize microscope operating conditions and interpret polymer image data.

ACKNOWLEDGEMENTS

The authors would like to thank their many collaborators: Steve Hudson (thermotropic liquid-crystal polyesters), Pete Haaland (AFM), Tim Bunning (siloxane cholesterics, polymer dispersed liquid crystals), Dwight Schwark and John Reffner (block copolymers), Jim Speck (ion-implanted PBO), and Hao Jiang and Soumya Patnaik (polyethylene single crystals). Thanks are due to Terry Reilly for taking the images in *Figure 19*. Special thanks go to Joe Williams for maintaining the microscope, and to David Joy for sharing his knowledge of SEM. DLV and ELT would like to acknowledge support from AFOSR Grants 910078 and F49 620-94-1-0224.

REFERENCES

1 White, J. R. and Thomas, E. L. *Rubber Chem. Technol.* 1984, **57**, 457
2 Everhart, T. E. and Thornley, R. F. M. *J. Sci. Instrum.* 1960, **37**, 246
3 Pawley, J. *J. Microsc.* 1984, **136**, 45
4 Goldstein, J. I., Newbury, D. E., Echlin, P., Joy, D. C., Fiori, C. and Lifshin, E. 'Scanning Electron Microscopy and X-Ray Microanalysis', Plenum, New York, 1981
5 Nagatani, T., Saito, S., Sato, M. and Yamada, M. *Scan. Microsc.* 1987, **1**, 901
6 Vezie, D. L. and Adams, W. W. *J. Mater. Sci. Lett.* 1990, **9**, 883
7 Butler, J. H. in 'Microbeam Analysis' (Ed. D. G. Howitt), San Francisco Press, San Francisco, 1991, p. 565
8 Drescher, H., Reimer, L. and Seidel, H. *Angew. Phys.* 1970, **29**, 331
9 Peters, K.-R. *Scan. Electron Microsc.* 1982, **IV**, 1359
10 Seiler, H. *J. Appl. Phys.* 1983, **54**, R1
11 Joy, D. C. *J. Microsc.* 1991, **161**, 343
12 Kanaya, K. and Okayama, S. *J. Phys. (D) Appl. Phys.* 1972, **5**, 43
13 Burke, E. A. *IEEE Trans. Nucl. Sci.* 1980, **NS-27**, 1760
14 Butler, J. H., Joy, D. C., Bradley, G. F., Krause, S. J. and Brown, G. M. *Microscopy: The Key Research Tool* 1992, p. 103
15 Vaz, O. W., MS. Thesis, Arizona State University, 1986
16 Price, C. W. and McCarthy, P. L. *Scanning* 1988, **10**, 29
17 Sawyer, L. C. and Grubb, D. T. 'Polymer Microscopy', Chapman and Hall, New York, 1987
18 Schwark, D. W., unpublished results, 1992
19 Reilly, T. Personal communication, 1989
20 Heide, H. G. *Lab. Invest.* 1965, **14**, 396
21 Grubb, D. T. *J. Mater. Sci.* 1974, **9**, 1715
22 Thomas, E. L. 'Structure of Crystalline Polymers', Elsevier Applied Science, London, 1984
23 Bahr, G. F., Johnson, F. B. and Zeitler, E. *Lab. Invest.* 1965, **14**, 377
24 Kobayashi, K. and Sakaoku, K. *Lab. Invest.* 1965, **14**, 359
25 Grubb, D. T., Keller, A. and Groves, G. W. *J. Mater. Sci.* 1972, **7**, 131
26 Grubb, D. T. and Keller, A. *J. Mater. Sci.* 1972, **7**, 822
27 Heavens, J. W., Keller, A., Pope, J. M. and Rowell, D. M. *J. Mater. Sci.* 1970, **5**, 53
28 Sutherland, R. L., Natarajan, L. V., Tondiglia, V. P. and Bunning, T. J. *Chem. Mater.* 1993, **5**, 1533
29 Sutherland, R. L., Tondiglia, V. P., Natarajan, L. V., Bunning, T. J. and Adams, W. W. *Appl. Phys. Lett.* 1994, **64**, 1074
30 Kawamoto, H., Yamazaki, S., Ishikawa, A. and Buchanan, R. *Scan. Electron Microsc.* 1984, **I**, 15
31 Hudson, S. D., Vezie, D. L. and Thomas, E. L. *Makromol. Chem., Rapid Commun.* 1990, **11**, 657
32 Campbell, F. W. and Maffei, L. *Sci. Am.* 1974, 106
33 Bunning, T. J., Vezie, D. L., Lloyd, P. F., Haaland, P. D., Thomas, E. L. and Adams, W. W. *Liq. Cryst.* 1994, **16**, 769
34 Schwark, D. W., Vezie, D. L., Reffner, J. R., Thomas, E. L. and Annis, B. K. *J. Mater. Sci. Lett.* 1992, **11**, 352
35 Berry, V. K. *Scanning* 1988, **10**, 19
36 Vezie, D. L., Ph.D. Thesis, Massachusetts Institute of Technology, 1993
37 Tarin, P. M. and Thomas, E. L. *Polym. Eng. Sci.* 1978, **18**, 472
38 Shimamura, K. *J. Macromol. Sci., Phys. (B)* 1979, **16**, 213
39 Shimamura, K., Murakami, S., Tsuji, M. and Katayama, K. *Nippon Reorji Gakkaishi* 1979, **7**, 42
40 Adams, W. W., Yang, D. and Thomas, E. L. *J. Mater. Sci.* 1986, **21**, 2239